The Compressive Behaviour of Mortar Under Varying Stress Confinement

A. Drougkas, E. Verstrynge & K. Van Balen
Building Materials and Building Technology Division
KU Leuven, Leuven, Belgium

ABSTRACT: The confinement of mortar in masonry under compression is one of the key processes influencing the compressive strength of the composite material. It is triggered by the mismatch of elastic properties between units and mortar, coupled with deformation conformity between the two material phases. In cases where the mortar is particularly deformable compared to the units, this confinement results in a peak stress many times the uniaxial compressive strength of the mortar. Therefore, a careful examination of this effect is critical in understanding the failure mechanisms of masonry in compression.
Mortar under compression can be modelled in a damage mechanics context, following the establishment of a) a constitutive stress-strain relation, b) a model for the increase of the compressive failure stress under lateral confinement and c) a model for the development (increase) of the Poisson's ratio of mortar under different stress levels. The first aspect is approached using established hardening-softening curves used for quasi-brittle materials, such as concrete. The second aspect is dealt with through the adoption of a suitable and sufficiently flexible failure criterion. The third aspect is addressed through fitting against experimental data.
The above aspects are expressed in a damage mechanics context, resulting in fast calculations of the compressive stress-strain curves for confined mortar. This approach allows the quantification of the development of damage in compression, the development of the apparent compressive strength and the relation between orthogonal strains in the mortar, leading to a full characterization of the stress, deformation and damage of the material. The analysis results are compared to experimental findings on different mortar types and are used for their interpretation and evaluation. The complexity of the behaviour of confined mortar is demonstrated, motivating the use of advanced numerical models for its accurate simulation and assessment.

1 INTRODUCTION

1.1 *State of the Art*

The compressive behaviour and strength of masonry is influenced by numerous geometric and material parameters. Chief among them is the behaviour of the mortar in the bed joints under the confinement effect imposed on it by the units. This effect is a function of the stresses acting in directions perpendicular to the direction of the compressive load. This confinement effect can lead to a substantial increase in the apparent compressive strength of the mortar in the joint, and therefore of the masonry composite.

When studying the behaviour of masonry in compression, the interaction of the units and the mortar is paramount in understanding and quantifying the confinement effect. From a numerical standpoint, the Poisson's ratio of the mortar is the chief property affecting the lateral expansion of the material. Since high compressive stress results in practically zero slip between the units and the mortar, displacement conformity can be assumed between the two phases of the masonry composite. This assumption forms the basis of many analytical models of unit/mortar interaction in masonry (Haller 1958, McNary and Abrams 1985).

This phenomenon is demonstrable using numerical means for the simulation of the masonry composite in compression, which highlight the role of the assumed Poisson's ratio in determining the ultimate stress and the failure mode (Drougkas et al. 2019). Nevertheless, measuring the Poisson's ratio in brittle cementitious materials, such as concrete and masonry mortars, is a difficult task (Mohamad et al. 2007, Ottosen 1979). This problem is compounded by the difficulty in distinguishing between the elastic component of the lateral deformation of the mortar under compression and the component resulting from plastic deformation. It is therefore necessary to also distinguish between the actual Poisson's ratio as a material parameter and the apparent Poisson's ratio as a measured quantity. The potentially substantial difference between the actual and apparent Poisson's ratios of mortar in masonry under compression (Drougkas et al. 2019) needs to be considered when determining the elastic properties of

mortar using, for example, electromechanical or optical measurements.

This distinction may be considered by adopting a damage mechanics approach in the behaviour of mortar in compression. By assigning a constitutive law for the development of the actual Poisson's ratio and calculating the apparent Poisson's ratio it is possible to study this complex effect in depth.

1.2 *Objectives*

In this paper a damage mechanics approach is developed in a numerical context and applied to available experimental data, aiming at simulating the behaviour of mortar in masonry joints. The main focus of the model is the simulation of the lateral expansion of the mortar under vertical loading, governed by a non-constant Poisson's ratio. A model for the development of the Poisson's ratio under different confinement is proposed.

The proposed model is tested against experimental data on cement mortars from the literature and against data from a recent testing campaign.

2 EXPERIMENTAL DATA

2.1 *Overview*

Two sets of experimental data are used for the validation of the proposed model: a) the experiments by McNary and Abrams (McNary and Abrams 1985) and b) the experiments by Hayen et al (Hayen et al. 2009), previously reported by Drougkas et al (Drougkas et al. 2019).

The first set, designated as 'Series 1', involves masonry mortars of the standard types M, S, N, O (ASTM 2019). Information on the lateral expansion of these mortars under different levels of confinement is provided for the M and O varieties, designated here as mortars M_1 and O_1.

The second set, designated 'Series 2', involves a similar series of masonry mortars, with variations on the type of lime and aggregate. Further experimental investigation is ongoing, with complete data on lateral expansion being currently available for one type of mortar under uniaxial compression, designated here as mortar O_2.

The mixtures of the mortars investigated in this paper are presented in Table 1. While not entirely conforming to the mix specifications of typical O mortars, the O_2 mortar had a similar uniaxial compressive strength and lateral expansion behaviour as O_1.

The experimentally obtained uniaxial compressive strength f_c and the Young's modulus E of these mortars are given in Table 2.

Overall, the two data sets do not provide full result data for lateral deformation of mortar under confinement. They have been performed with different materials, different procedures and the results are presented in different ways. However, it was deemed desirable to attempt the application of the proposed model to as large a number of cases as possible.

Table 1: Summary of mortar mixtures per weight: cement (C), lime (L), sand (S) and water-to-cement ratio ($W:C$).

Mortar	C	L	S	$W:C$
M_1	1.00	0.25	3.00	0.55
O_1	1.00	2.00	9.00	1.96
O_2	1.53	1.00	11.86	1.85

Table 2: Uniaxial compressive strength and Young's modulus of mortars.

	f_c (N/mm^2)	E (N/mm^2)
M_1 mortar	31.1	11600
O_1 mortar	6.2	1750
O_2 mortar	5.0	713

The stresses applied on the samples may be normalized using two different approaches. The confining stresses $\sigma_x = \sigma_z = \sigma_c$ can be normalized through division by the vertically applied stress σ_y. The applied vertical stress itself may be normalized by division by the confined compressive strength f_{cc} registered for each level of stress confinement. These normalizations are given by the expressions:

$$\beta_1 = \left|\frac{\sigma_c}{\sigma_y}\right| \qquad \beta_2 = \left|\frac{\sigma_y}{f_{cc}}\right| \tag{1}$$

Both normalized parameters assume values between 0.0 and 1.0 and are meaningful for any level of confinement. Absolute values are considered in the normalization since compressive stresses are negative while tensile forces and material properties, such as f_{cc}, are positive.

The initial and final apparent Poisson's ratio, defined at the beginning of loading and at peak stress respectively, are designated ν_i and ν_f. While the behaviour of masonry in compression is heavily influenced by the Poisson's ratio throughout the loading process, ν_f is the parameter that has the greatest influence in the peak load.

2.2 *Series 1 mortar*

For the study of the Poisson's ratio of masonry mortar in compression, the results of the experiments by McNary are investigated (McNary and Abrams 1985). This set of results includes four mortars with different elastic and strength properties under different levels of lateral stress confinement. Details on the measured apparent Poisson's ratio are given for two of these mortars.

In addition to uniaxial testing, the mortars were subjected to compression under different levels of lateral stress confinement. This confinement was provided by testing cylindrical samples in a Hoek cell, which provides uniform lateral stress confinement. Deformation measurements were acquired, providing information on the samples' apparent Poisson's ratio.

The apparent Poisson's ratio $\hat{\nu}$ is plotted against the normalized applied vertical stress β_2 for different levels of lateral compression σ_c in Figure 1. No information on the scatter is provided. For all cases, the initial Poisson's ratio is very low, roughly around 0.10, and increases for higher values of vertical load. This increase leads the Poisson's ratio to assume values higher than what normally admissible in elasticity. Additionally, it is immediately apparent that for the same lateral confining stress, the M_1 mortar presents a generally higher apparent final Poisson's ratio than the O_1 mortar. The reason for this is not clear, but could potentially be linked to the higher porosity of the O_1 mortar, which results in lower lateral expansion due to pore collapse in compression.

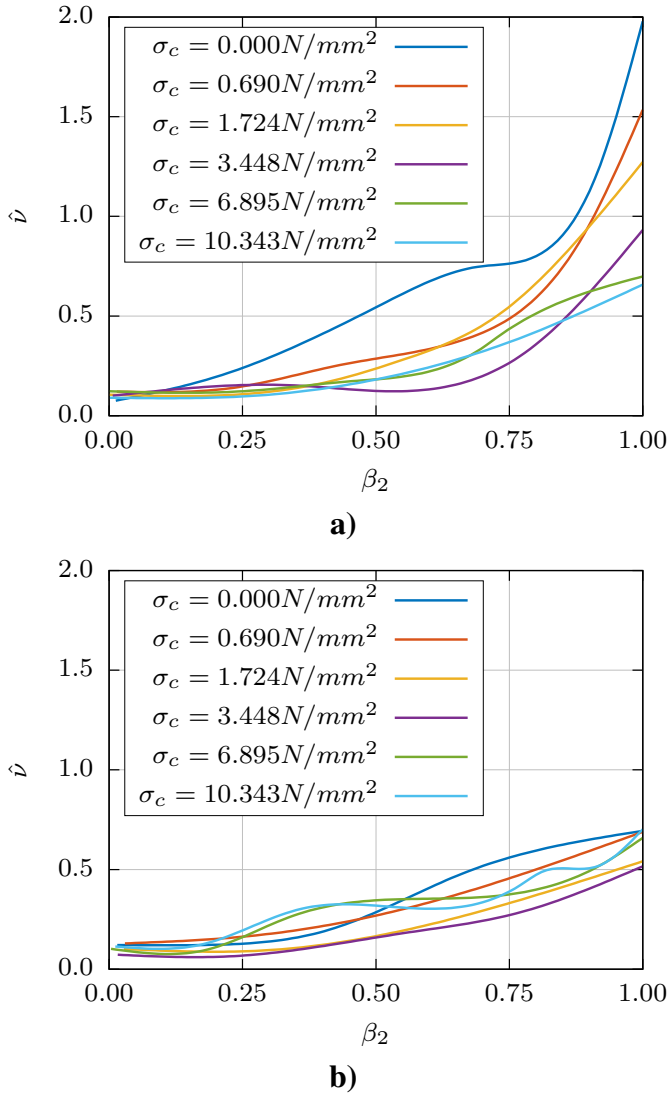

Figure 1: Experimentally determined apparent Poisson's ratio of a) mortar M_1 and b) mortar O_1 (adapted from McNary and Abrams 1985).

2.3 *Series 2 mortar*

Data on the O_2 mortar is limited as the lateral expansion behaviour of the material has only been tested in uniaxial loading conditions in cylindrical samples. However, the data acquired from the test is valuable in this investigation.

Three samples of the same material were tested in uniaxial compression, and the resulting apparent Poisson's ratio is shown in Figure 2. The behaviour of this mortar is distinctly different from that of the Series 1 mortars. The initial Poisson's ratio is negligible and the lateral expansion under compression is only mobilized at around 50% of the peak load. However, the final Poisson's ratio is similar to the one obtained for the O_1 mortar, which has similar compressive strength and Young's modulus.

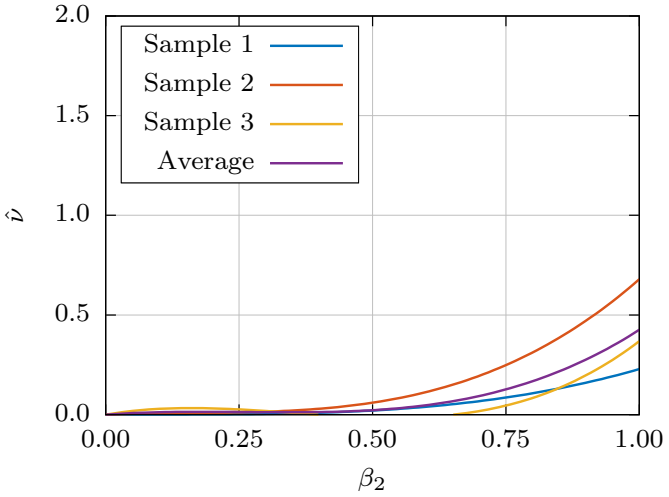

Figure 2: Apparent Poisson's ratio of O_2 mortar.

Additional triaxial compression tests were conducted on the O_2 mortar. The obtained confined compressive strength f_{cc} and peak strain ε_{cc} are reported in Table 3.

Table 3: Triaxial compressive test results for O_2 mortar.

β_1 (−)	f_{cc} (N/mm^2)	E (N/mm^2)	ε_{cc} (‰)
0.00	5.25	712.7	12.66
0.05	8.68	937.9	23.74
0.10	11.40	1296.7	32.34
0.15	12.96	1168.0	34.02
0.25	15.94	1134.5	43.21

3 NUMERICAL MODEL

3.1 *Overview*

The mortar samples are modelled using a simple model for the stress and strain state of the material. This model simulates the stress state in the mortar under uniform triaxial compression, as it arises in a Hoek cell. While stresses through the volume of the

mortar in a masonry joint may not be constant, especially near the free edges of the joint, they assume relatively uniform values for a substantial proportion of their volume around the centre of the joint (Drougkas, Roca, & Molins 2015). Therefore, the approach of uniform confinement adopted here is considered adequate for the simulation of mortar in masonry joints.

3.2 *Basic expressions*

The three-dimensional Hooke's law is used for relating the effective stress tensor σ with the strain tensor ε. Disregarding shear stresses, its matrix form reads:

$$\begin{bmatrix} \varepsilon_x \\ \varepsilon_y \\ \varepsilon_z \end{bmatrix} = \frac{1}{E} \begin{bmatrix} 1 & -\nu & -\nu \\ -\nu & 1 & -\nu \\ -\nu & -\nu & 1 \end{bmatrix} \begin{bmatrix} \sigma_x \\ \sigma_y \\ \sigma_z \end{bmatrix} \tag{2}$$

where E is the Young's modulus and ν is the actual Poisson's ratio. The term effective stress signifies the stress that is proportional to the strain and is different from the actual stress. Positive values for stress and strain indicate tension.

The actual stress in compression is calculated through the use of a parabolic stress-strain curve based on fracture energy proposed for concrete (Feenstra and Borst 1996). The increase of the compressive strength due to confinement is taken into account through the use of the Hsieh-Ting-Chen failure criterion (Hsieh et al. 1982). This criterion, based on four numerical parameters derived from different experimental tests, affords substantial flexibility in the definition of the desired failure criterion and can be degenerated to other failure curves, such as the Drucker-Prager criterion. Finally, the variation of the Poisson's ratio of mortar as a function of applied load is modelled using a semi-empirical expression (Drougkas et al. 2019).

Adopting a damage mechanics approach for compression, the actual, or damaged, stress is related to the effective stress from eq. 2 through the use of an integrity variable. According to the constitutive law chosen for compression (negative stress), this variable is calculated according to the piecewise parabolic equation (Drougkas et al. 2019):

$$C(\varepsilon) = \begin{cases} 1 & if \quad 0 \le \varepsilon \le \varepsilon_l \\ -\frac{f_c}{\sigma} \left(\begin{array}{c} \frac{1}{3} + \frac{4}{3} \frac{\varepsilon - \varepsilon_l}{\varepsilon_c - \varepsilon_l} - \\ \frac{2}{3} \left(\frac{\varepsilon - \varepsilon_l}{\varepsilon_u - \varepsilon_l} \right)^2 \end{array} \right) & if \quad \varepsilon_l \le \varepsilon \le \varepsilon_c \\ -\frac{f_c}{\sigma} \left(1 - \left(\frac{\varepsilon - \varepsilon_c}{\varepsilon_u - \varepsilon_c} \right)^2 \right) & if \quad \varepsilon_c \le \varepsilon \le \varepsilon_u \\ 0 & if \quad \varepsilon_u \le \varepsilon \end{cases} \tag{3}$$

where f_c is the compressive strength, ε is the strain and σ is the effective stress in the direction being evaluated. The actual stress tensor σ_d is derived from σ through:

$$\sigma_d = \sigma C(\varepsilon) \tag{4}$$

Damage is isotropic, meaning that reduction of stiffness due to damage in one direction leads to the same reduction in stiffness in all loading directions. The strain ε_l is the limit of proportionality in compression:

$$\varepsilon_l = -\frac{1}{3} \frac{f_c}{E} \tag{5}$$

ε_c is the peak strain:

$$\varepsilon_c = -\frac{5}{3} \frac{f_c}{E} \tag{6}$$

and ε_u is the ultimate strain:

$$\varepsilon_u = \varepsilon_c - \frac{3}{2} \frac{{G_f}^c}{f_c l} \tag{7}$$

where ${G_f}^c$ is the compressive fracture energy and l is the characteristic length, here equal to the sample height, which only affects the post-peak part of the stress-strain curve.

3.3 *Triaxial Confinement of Mortar*

The failure criterion, expressed in principal stress terms, reads:

$$f = A \frac{J_2}{{f_c}^2} + B \frac{\sqrt{J_2}}{f_c} + C \frac{\sigma_1}{f_c} + D \frac{I_1}{f_c} - 1 \tag{8}$$

where I_1 and J_2 are the first stress and second deviatoric stress invariants respectively, expressed as:

$$\begin{aligned} I_1 &= \sigma_1 + \sigma_2 + \sigma_3 \\ J_2 &= \frac{1}{6} \left((\sigma_1 - \sigma_2)^2 + (\sigma_2 - \sigma_3)^2 + (\sigma_3 - \sigma_1)^2 \right) \end{aligned} \tag{9}$$

and σ_1 is the maximum of the principal stresses σ_1, σ_2 and σ_3. The numerical parameters A, B, C, D are calculated by solving a linear system of equations derived from eq. 8 for 4 different types of loading: uniaxial compression, uniaxial tension, biaxial compression and triaxial compression. The confined compressive strength f_{cc} is calculated by solving eq. 8 for the given laterally applied confinement stresses.

The increase in the peak stress due to confinement also results in an increase in the peak strain. This increase is calculated according to the Eurocode 2 expression for concrete (CEN 2004):

$$\varepsilon_{cc} = \varepsilon_c \left(\frac{f_{cc}}{f_c} \right)^2 \tag{10}$$

The equation for the ultimate strain ε_u remains unchanged. This results in a more brittle post-peak response for confined mortar, as the energy expended between peak and ultimate strain does not change.

3.4 *Poisson's Ratio*

For the actual Poisson's ratio ν, the following equation, a function of the applied vertical stress, is here proposed:

$$\nu(\beta_2) = (\nu_f - \nu_i)\,{\beta_2}^3 + \nu_i \tag{11}$$

where ν_i and ν_f are the initial and final Poisson's ratios, the latter registered at peak stress. For the Series 1 mortars examined in this paper, a value of 0.10 is taken for ν_i, while 0.00 is considered for the Series 2 mortar. The value of ν_f is, in turn, expressed as:

$$\nu_f(y) = y(t)\,\frac{f_{cc}}{f_c} \tag{12}$$

where y is the vertical abscissa of a quadratic Bézier curve and t is its time parameter, tracing the curve from beginning to end through variation from 0 to 1. The horizontal abscissa x is:

$$x = \varepsilon_{cc} \tag{13}$$

while for $y(t)$ the piecewise equation is proposed:

$$y(t) = \begin{cases} y_1 & if \quad 0 \le x \le x_2 \\ (1-t)\left((1-t)\,y_1 + y_2 t\right) & if \quad x_2 \le x \le x_3 \\ \quad +t\left((1-t)\,y_2 + y_3 t\right) & \\ y_3 & if \quad x_3 \le x \end{cases} \tag{14}$$

Inversely to the way in which Bézier curve equations are normally expressed, the time parameter t is expressed as a function of the horizontal abscissa x as:

$$t(x) = \frac{\sqrt{(x-x_1) + {x_2}^2 + x(x_1 - 2x_2)} - x_2 + x_1}{x_3 - 2x_2 + x_1} \tag{15}$$

The value of $t(x)$ can be plugged into eq. 14 in order to obtain the value of the vertical abscissa.

In its quadratic form, a Bézier curve is characterized by three control points: a starting point $P_0(x_0, y_0)$, an intermediate point $P_1(x_1, y_1)$ and an end point $P_2(x_2, y_2)$. The curve connects the end points P_0 and P_2, while P_1 serves as a control point, which does not necessarily lie on the curve. Bézier curves allow for enhanced flexibility and mathematical convenience in interpolating experimental data compared to polynomial curves. Further, the numerical parameters of the curve, namely the abscissae of the control points, can be directly related to the physical parameters being modelled and evaluated. Hence the adoption of this approach in this paper.

The coordinates for the Bézier curve control points for fitting the experimental data are presented in Table 4.

Table 4: Coordinates of control points for actual Poisson's ratio of mortar ν model.

x_0	0.005	y_0	2.000
x_1	0.005	y_1	0.200
x_2	0.025	y_2	0.200

3.5 *Analysis Procedure*

For a linear elastic analysis the relevant material properties and applied stresses or strains can be simply plugged in eq. 2 and solving the system of linear equations. In the case of a non-linear analysis, the system of equations is solved in steps of applied strain in the vertical y direction. The system of equations $F(X_n)$ is solved iteratively for each load step using a Newton algorithm:

$$X_{n+1} = X_n - J_F(X_n)^{-1}\,F(X_n) \tag{16}$$

where n is the iteration number and $J_F(X_n)$ is the Jacobian matrix. The variables assembled in the X_n tensor are the stresses, strains, integrity variables in compression and the actual Poisson's ratio of the material as previously defined in the description of the analytical model.

Due to the analytical formulation of the problem using a small system of simple linear equations, the non-linear analysis can be executed with very low computational cost.

In the first iteration of every load step, the integrity variable and Poisson's ratio of the previous step is used. At every subsequent iteration executed, trial values are calculated for the integrity variable C and the Poisson's ratio ν according to the stress and strain increment. These trial values are compared with the initial values for which the iteration is executed. The convergence criterion is considered satisfied when the trial and actual values differ by less than 0.1%. For applied strain load steps equal to 0.0001, convergence is typically reached within 15 iterations.

From eq. 11 it is possible to determine the actual Poisson's ratio ν of the material. The apparent Poisson's ratio is calculated in the analysis according to the standard definition of the negative ratio of lateral over vertical deformation:

$$\hat{\nu} = -\frac{\varepsilon_x}{\varepsilon_y} \tag{17}$$

In the absence of relevant data, the compressive fracture energy is given a nominal value, calculated as (Drougkas et al. 2015):

$$G_f{}^c = f_c d \tag{18}$$

where d is a ductility index equal to $1mm$.

4 NUMERICAL ANALYSIS RESULTS

4.1 *Overview*

The predictive capacity of the proposed model for the final apparent Poisson's ratio is checked. The results of the analytical models compared to the experimental data are presented in Figure 3. Good overall coincidence is obtained between the piecewise expression and the experimental data.

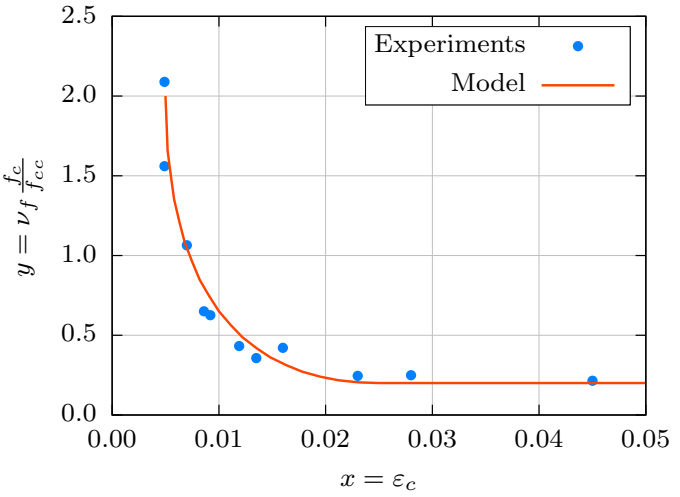

Figure 3: Comparison of analytical model for ν_f with experimental data for M_1, O_1 and O_2 mortars.

4.2 *Series 1 mortars*

Initially, the assumption for the increase in the peak strain due to confinement according to eq. 10 is checked. The experimentally determined stress-strain graphs of the M_1 and O_1 mortars and their comparison with the model results are presented in Figure 4.

While the experimentally determined curves for the O_1 mortar are not completely reported, a good match is obtained for the O_1 mortar up to the peak. The very short post-peak response reported in the O_1 mortar tests indicates that a lower value for the compressive fracture energy should be used. However, conclusive remarks cannot be made in this aspect due to the absence of a complete post-peak curve from the tests as reported. Therefore, no adjustment was deemed necessary at this point.

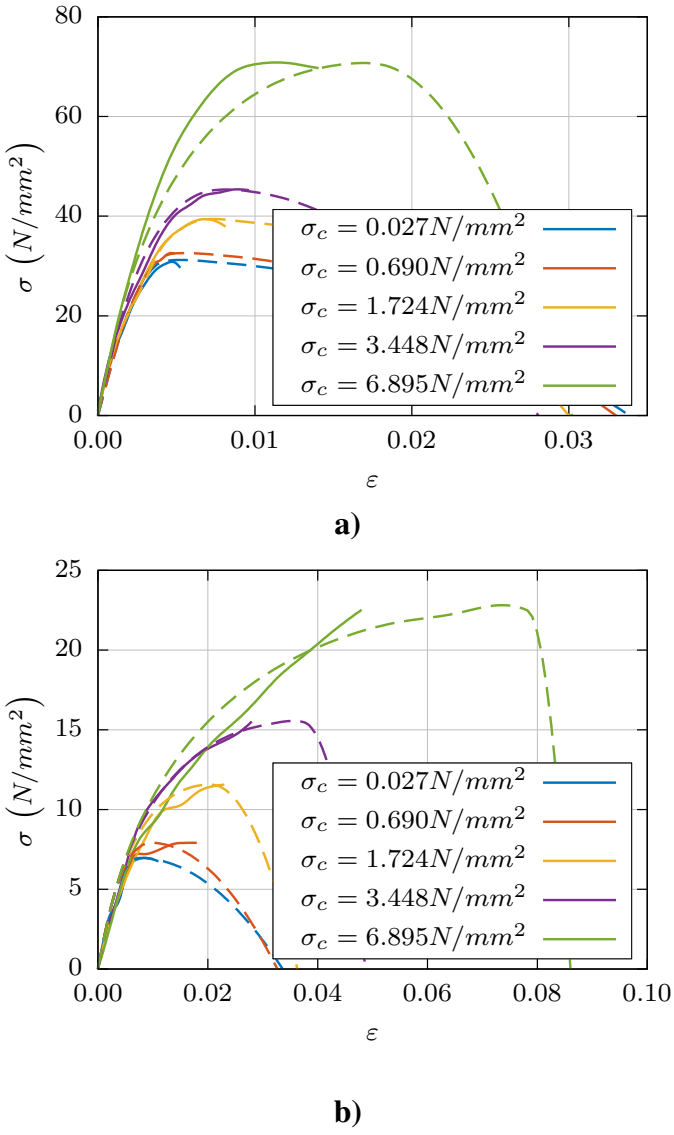

Figure 4: Comparison of experimentally determined (solid lines) and numerically derived (dashed lines) stress-strain curves: a) mortar M_1 and b) mortar O_1 (experimental data adapted from McNary and Abrams 1985).

The comparison of the experimentally determined and numerical derived apparent Poisson's ratio is presented in Figure 5. The model is able to calculate the initial and final apparent Poisson's ratio of the mortar with good accuracy for most cases, while intermediate values are captured well in the cases where the experimental behaviour presents a regular pattern. It successfully captures the overall difference in the resulting values between the two types of mortar in Series 1.

4.3 *Series 2 mortar*

The stress-strain curves obtained experimentally and numerically for the O_2 mortar are compared in Fig-

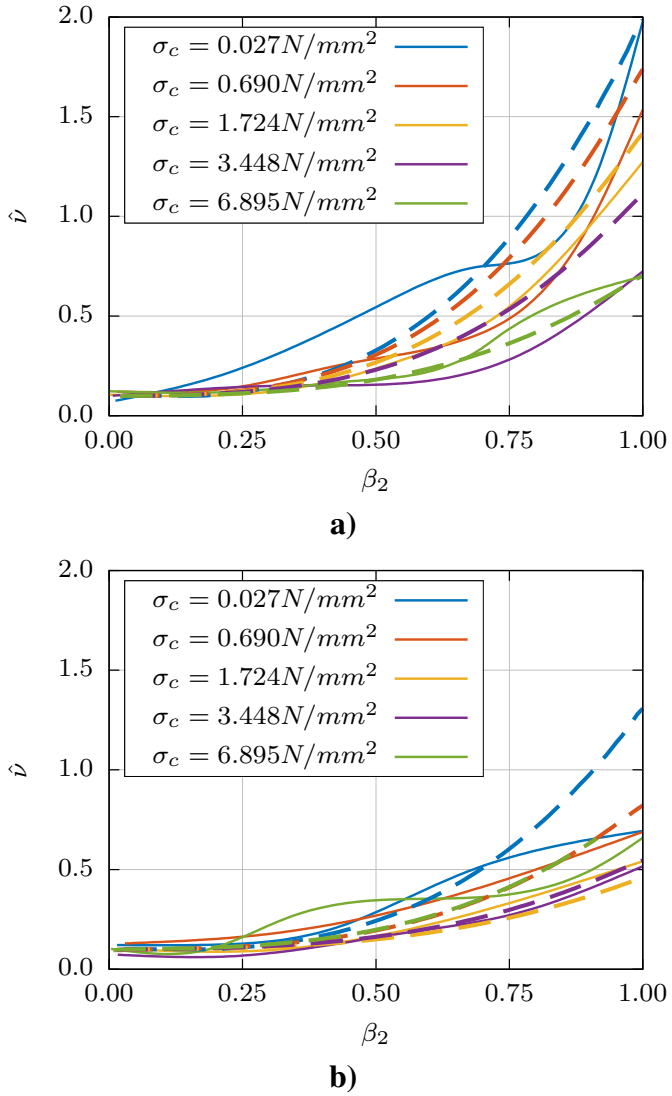

Figure 5: Comparison of experimentally determined (solid lines) and numerically derived (dashed lines) apparent Poisson's ratio: a) mortar M_1 and b) mortar O_1.

ure 6. The compressive fracture energy used in the model was calculated as for the Series 1 mortars, with a very good fit being obtained in this case with the experimental data. More importantly, the peak strain has been calculated with good accuracy and a complete post-peak curve has been registered.

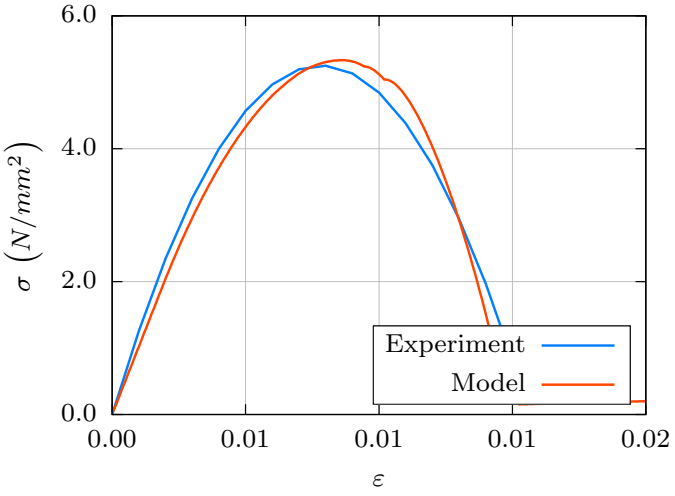

Figure 6: Comparison of experimental and numerically derived stress strains curves for O_2 mortar.

The proposed model is additionally evaluated in terms of predicted Poisson's ratio compared to the experimental average. This comparison is illustrated in Figure 7. Assuming a value of 0.00 for ν_i, a good prediction of the behaviour of the mortar is obtained, mainly in terms of ν_f at peak load. According to the proposed model, the value elected for ν_i does not affect the ν_f parameter, and therefore has no real influence on the peak load. It may, nevertheless affect the mode of damage initiation in the masonry composite.

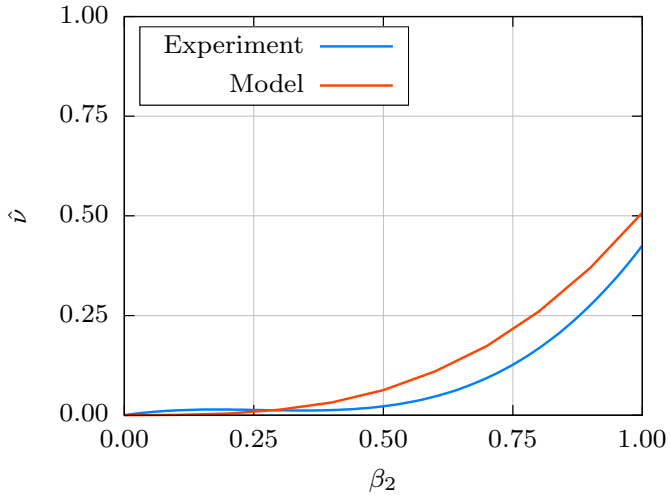

Figure 7: Comparison of analytical model for ν_f with experimental data for O_2 mortar.

Finally, the numerically calculated confined compressive strength f_{cc} and peak strain ε_{cc} are presented in Table 5. An excellent approximation of both values is achieved for nearly the entire range of β_1 investigated in the experiments (compare with Table 3). The only notable discrepancy is obtained for a value $\beta_1 = 0.25$, where a lower than anticipated peak strain was obtained in the experiments.

Table 5: Numerical results for O_2 mortar: compressive strength and peak strain under confinement.

β_1 $(-)$	f_{cc} (N/mm^2)	ε_{cc} $(‰)$
0.00	5.25	11.88
0.05	6.66	25.50
0.10	8.26	32.34
0.15	10.30	30.14
0.25	16.10	68.00

5 CONCLUSIONS

A model for the development of the Poisson's ratio of mortar under compression is proposed. It is implemented in a numerical damage mechanics context and compared to relevant experimental results. The model accounts for the shift in compressive behaviour and lateral expansion of mortar under different levels of

stress confinement. A variety of mortar types are investigated, the main characteristics of their response being successfully captured by the model.

The distinction between the Poisson's ratio of mortar as a material property and as an apparent value is important. While differences in the two parameters in stand-alone samples may not be substantial, the differences in masonry joints need to be considered.

Further work focusing on lime-based mortars is required. Confinement effects are more pronounced in masonry made with deformable mortars with low or zero cement content due to the increased relative deformability of the mortar compared to the units. The initial Poisson's ratio may also be substantially different from the values encountered in cement mortars due to differences in porosity.

REFERENCES

ASTM (2019). *ASTM C 270 - Standard Specification for Mortar for Unit Masonry*.

CEN (2004). *EN 1992-1-1 - Eurocode 2: Design of concrete structures - Part 1-1: General rules and rules for buildings*.

Drougkas, A., P. Roca, & C. Molins (2015). Numerical prediction of the behavior, strength and elasticity of masonry in compression. *Engineering Structures 90*, 15–28.

Drougkas, A., E. Verstrynge, R. Hayen, & K. Van Balen (2019). The confinement of mortar in masonry under compression: Experimental data and micro-mechanical analysis. *International Journal of Solids and Structures 162*(May), 105–120.

Feenstra, P. H. & R. D. Borst (1996). A composite plasticity model for concrete. *International Journal of Solids and Structures 33*(5), 707–730.

Haller, P. (1958). Hochhausbau in Backstein: die technischen Eigenschaften von Backstein-Mauerwerk für Hochhäuser. *Schweizerische Bauzeitung 76*(28), 411–419.

Hayen, R., K. Van Balen, & D. Van Gemert (2009). Triaxial interaction of natural stone, brick and mortar in masonry constructions. *Building Materials and Building technology to Preserve the Built Heritage, WTA Schriftenreihe*, 333–352.

Hsieh, S. S., E. C. Ting, & W. F. Chen (1982). A plastic-fracture model for concrete. *International Journal of Solids and Structures 18*(3), 181–197.

McNary, W. S. & D. P. Abrams (1985). Mechanics of Masonry in Compression. *Journal of Structural Engineering 111*(4), 857–870.

Mohamad, G., P. Lourenço, & H. R. Roman (2007). Mechanics of hollow concrete block masonry prisms under compression: Review and prospects. *Cement and Concrete Composites 29*(3), 181–192.

Ottosen, N. S. (1979). Constitutive Model for Short-Time Loading of Concrete. *Journal of the Engineering Mechanics Division 105*(1), 127–141.